Thermal conductivity of a kind of mesoporous silica SBA-15*

Huang Cong-Liang(黄丛亮)[a], Feng Yan-Hui(冯妍卉)[a]†, Zhang Xin-Xin(张欣欣)[a], Li Jing(李 静)[a], and Wang Ge(王 戈)[b]

[a] School of Mechanical Engineering, University of Science and Technology Beijing, Beijing 100083, China
[b] School of Materials Science and Engineering, University of Science and Technology Beijing, Beijing 100083, China

(Received 29 August 2012; revised manuscript received 23 October 2012)

Mesoporous silica SBA-15 consists of uniform hexagonal, unconnected cylindrical channels with diameters that can be tuned within a range of 1.5 nm–30 nm, and is thought to have a special thermal conductivity. The theoretical investigation of the shell thermal conductivity of the mesoporous silica is performed in the relaxation time approximation in this paper and an available one-dimensional heat transfer model is used to predict the effective thermal conductivity (ETC) of the mesoporous silica. The experimental result of the ETC is also presented for comparison. The shell thermal conductivity of the mesoporous silica decreases with mesochannel radius increasing or wall thickness decreasing, but does not strictly decrease with porosity increasing. The thermal radiation possibly plays a primary role in heat transfer at the large porosity scale. The predicted ETC of SBA-15 with only conduction considered is quite low at the large porosity, even lower than the thermal conductivity of the silica aerogels. To realize it, doping carbon or other matters which can strongly absorb infrared light into SBA-15 is a possible way.

Keywords: mesoporous silica, thermal conductivity, SBA-15

PACS: 44.30.+v, 61.43.Gt **DOI:** 10.1088/1674-1056/22/6/064401

1. Introduction

Materials with either high or low thermal conductivities have attracted much attention since they have many potential applications in the areas such as liquid hydrogen launch vehicle tanks,[1] space launch applications,[2] solar hot-water collectors,[3] and heat exchangers,[4] and so on. Compared with widely studied silica aerogels which possesses quite a low thermal conductivity, the mesoporous silica is thought to be applicable to load nanomaterials, such as metallic nanoparticles,[5] nanowires,[6] polymers[7] or carbon,[8] within the mesochannels. Over the past 15 years, there has been a dramatic increase in the literature dealing with design, synthesis, characterization, and property evaluation of the mesoporous silicas for catalysis, adsorption, and separation. Although some investigations on the thermal conductivity of the mesoporous silica were reported,[9,10] it has not been systemically studied yet.

In this paper, we focus on the mesoporous silica SBA-15 to study its shell thermal conductivity by theoretical investigation under the relaxation time approximation and its effective thermal conductivity based on the available model combining the thermal conductivity of the shell and that of the confined air in mesochannels. The present work is expected to provide some useful information for the design of the mesoporous composites and their promising applications on the electronic and mechanical devices.

2. Nanostructure of the highly ordered mesoporous silica

SBA-15 with ordered mesochannels whose diameters are in a range of 1.5 nm–30 nm[11] is a two-dimensional hexagonal (space group *p6mm*) mesoporous silica, as shown in Fig. 1. Bright cells are channels separated by dark shells.

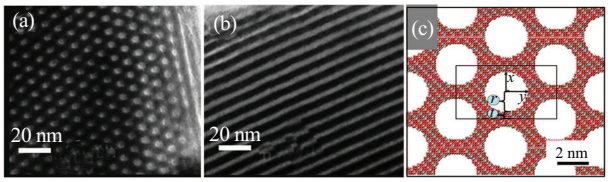


Fig. 1. (color online) Transmission electron microscopy (TEM) images: (a) cross section of channels in SBA-15,[12] (b) SBA-15 in the direction of the channel axis,[12] and (c) schematic nanostructure of the cross section of channels (Dark and bright spheres represent oxygen and silicon atoms, respectively).

3. Lattice thermal conductivity of the shell

While SBA-15 was thought to be a crystal material,[13] the regular bulk formula for the lattice thermal conductivity using the relaxation-time methods through the following Klemen's and Callaway's derivation is used in this paper, as shown in Refs. [14] and [15]:

$$k_{\mathrm{ph}} = \frac{k_{\mathrm{B}}}{2\pi^2 v}\left(\frac{k_{\mathrm{B}}T}{\hbar}\right)^3 \int_0^{\theta_{\mathrm{D}}/T} \frac{\tau_{\mathrm{c}} x^4 \mathrm{e}^x}{(\mathrm{e}^x - 1)^2}\,\mathrm{d}x, \tag{1}$$

*Project supported by the National Basic Research Program of China (973 Program) (Grant No. 2012CB720404), the National Natural Science Foundation of China (Grant No. 50836001), the FOK Ying Tong Education Foundation, China (Grant No. 121055), and the Fundamental Research Funds for the Central Universities, China (Grant Nos. FRF-AS-12-002 and FRF-TP-11-001B).

†Corresponding author. E-mail: yhfeng@me.ustb.edu.cn

© 2013 Chinese Physical Society and IOP Publishing Ltd

where k_B is the Boltzmann constant, h the Planck constant, θ_D the Debye temperature, τ_c the combined relaxation time, T the temperature, and v the average sound velocity, $x = (\hbar\omega)/(k_B T)$, and ω is the phonon frequency in radians per second.

The combined phonon relaxation time is obtained from the Matthiessen rule[16]

$$\frac{1}{\tau_c} = \frac{1}{\tau_U} + \frac{1}{\tau_M} + \frac{1}{\tau_{ph-e}} + \frac{1}{\tau_B}, \tag{2}$$

where τ_U, τ_M, τ_{ph-e}, and τ_B are relaxation times due to the anharmonic nature of the crystal potential enenrgy (three-phonon Umklapp sacttering), the mass-difference scattering, acoustic phonons scattered by electrons, and the boundary scattering, respectively.

The relaxation time for Umklapp scattering at a high temperature (room temperature and above) was given by Klemens[17,18] as

$$\frac{1}{\tau_U} = 2\gamma^2 \frac{k_B T}{\mu V_0} \frac{\omega^2}{\omega_D}, \tag{3}$$

where γ is the Grüneisen constant, ω_D the Debye frequency, V_0 the volume of the molecular, μ the shear modulus which can be estimated from the formula $\mu = v_t^2 \rho$, v_t the transverse sound velocity and ρ the density of the mesoporous silica.

Mass-difference scattering is the scattering of phonons due to differences in mass. The phonon relaxation rate on point defects is calculated using the following expression:[19]

$$\frac{1}{\tau_M} = \frac{V_0 \omega^4}{4\pi v^3} \Gamma, \tag{4}$$

where Γ is the measure of the strength of the mass-difference scattering.

The relaxation time for acoustic phonons scattered by electrons is given by[20]

$$\frac{1}{\tau_{ph-e}} = \frac{n_e \varepsilon^2 \omega}{\rho v^2 k_B T} \sqrt{\frac{\pi m^* v^2}{2 k_B T}} \exp\left(-\frac{m^* v^2}{2 k_B T}\right), \tag{5}$$

where n_e is the concentration of conduction electrons, ε the deformation potential, and m^* the electron effective mass. Because n_e and ε are difficult to determine for silica, the fitting method is used to contain the adaptable value of $n_e \varepsilon^2$. The result is shown in Fig. 2. As the value of $n_e \varepsilon^2$ is between 7.5×10^{-12} J·m^{-3} and 1.0×10^{-11} J·m^{-3}, thermal conductivities of the bulk silica calculated by Eq. (1) could accord quite well with the experimental results[21–23] in a range 100 K $\leq T \leq$ 500 K. Accordingly, the average value of $n_e \varepsilon^2$, i.e. 8.75×10^{-12} J·m^{-3}, is employed in this paper.

The boundary scatterings in both of the solid nanowire[19,24] and the hollow nanowire[25] are usually treated by applying the Casimir limit. That is, all phonons each with a positive normal velocity lose the sense of their directionality and obey the equilibrium distribution at the boundary. Obviously, in this paper, the mean free paths along the different directions are unalike. Thus, the possible maximum free path of phonons along the out of plane direction (the direction, which is along the axis of the channel in Fig. 1(c)) is similar to that of a hollow nanowire.[25] Similarly, the effective boundary mean free path can be written as

$$\lambda_Z = 2\sqrt{(r+t)^2 - r^2} \cdot \frac{t}{r}, \tag{6}$$

where t/r is the curvature of the wall to correct the possible maximum free path, r is the radius of mesochannel and t the half the wall thickness shown in Fig. 1(c). The surface of the channel is thought to be perfectly rough. So the boundary relaxation rate along the Z direction can be expressed as

$$\frac{1}{\tau_{B,Z}} = \frac{v}{\lambda_Z} = \frac{v}{2\sqrt{(r+t)^2 - r^2}} \cdot \frac{r}{t}. \tag{7}$$

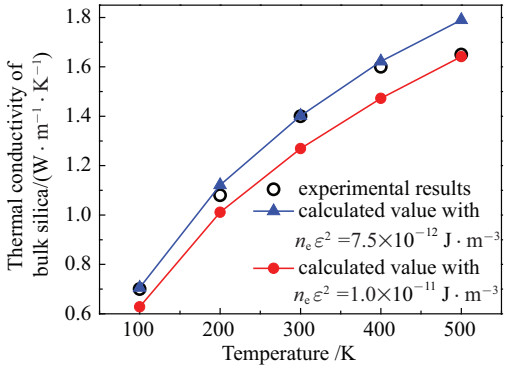


Fig. 2. (color online) Calculated thermal conductivities of the bulk silica with different values of $n_e \varepsilon^2$, and are compared with the experimental results.

While phonon flow acts in a manner similar to the way a fluid behaves, the possible maximum free path in the x–y plane (shown in Fig. 1(c)) is assumed to be the equivalent diameter of the mesochannel

$$\lambda_{xy} = \frac{2\sqrt{3}(r+t)^2 - \pi r^2}{2\pi r}. \tag{8}$$

Since the scattering probability of a phonon rises with r increasing or t decreasing,[25] we assume that the equivalent diameter should be multiplied by a correction factor t/r, which is the curvature of the wall. Therefore, it is reasonable to take the effective boundary mean free path in the x–y plane as

$$\lambda_{xy} = \frac{2\sqrt{3}(r+t)^2 - \pi r^2}{2\pi r} \cdot \left(\frac{t}{r}\right). \tag{9}$$

Accordingly, the boundary relaxation rate in the x–y plane can be written as

$$\frac{1}{\tau_{B,xy}} = \frac{v}{\lambda_{xy}} = \frac{2\pi r v}{2\sqrt{3}(r+t)^2 - \pi r^2} \cdot \left(\frac{r}{t}\right). \tag{10}$$

The parameters used in the calculation are summarized in Table 1.

Table 1. Parameters used in the calculation.

Parameter	Value	Reference
Density of mesoporous silicas ρ/g·cm^{-3}	2.2	[26]
Grüneisen's constant γ	0.45	[27]
Transverse sound velocity v_t/(m/s)	3.75×10^3	[28]
The average velocity of sound v/(m/s)	4.467×10^3	[28]
Debye temperature θ_D/K	511	[29]
Mass-difference scattering parameter Γ	1	[30]
Electron effective mass $m^*/(m_0)$	0.26	@
Volume of the molecular V_0/m^{-3}	3.76×10^{-29}	[30]

@ Since the electron effective mass of silica is not available, the electron effective mass was used here.

4. Discussion of lattice thermal conductivity of the shell

The shell thermal conductivities of the mesoporous silica with different values of radius r and different values of wall thickness $2t$ are studied at $T = 300$ K. The results are shown in Figs. 3(a) and 3(b). We can see that the smaller the wall thickness or the larger the radius of the channel, the lower the thermal conductivity of the mesoporous silica becomes. The shell thermal conductivity of the mesoporous silica gradually decreases to a constant value with the radius of the mesochannel increasing, if the wall thickness is kept constant. On the other hand, the shell thermal conductivity increases with wall thickness increasing, with the mesochannel radius kept constant. Furthermore, with the increase of radius, the thermal conductivity of the mesoporous silica with a larger wall thickness drops off more rapidly than that with a smaller one. The thermal conductivity in the X–Y plane is generally lower than that along the Z direction except for the case of small radius conditions like $r = 2$ nm.

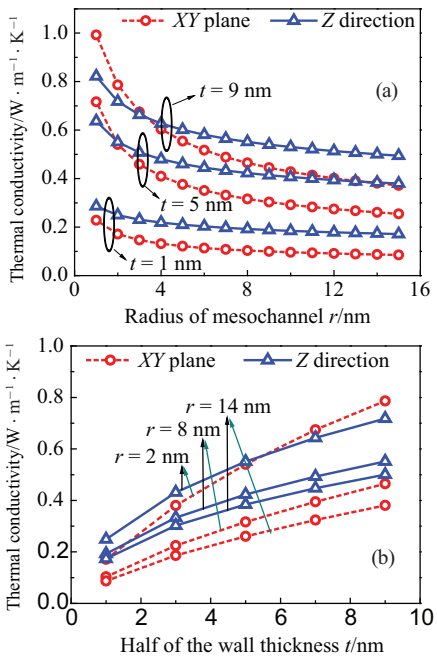


Fig. 3. (color online) Lattice thermal conductivities of the mesoporous silicas at $T = 300$ K (a) with different radii of mesochannel and (b) with different values of wall thickness.

In addition to the effects of the mesochannel radius and the wall thickness, the dependence of the thermal conductivity on the porosity is further considered. The porosity of the mesoporous silica can be calculated by

$$\phi = \frac{\pi r^2}{2\sqrt{3}\,(r+t)^2}. \tag{11}$$

From Eq. (11), it can be drawn that the porosity depends on the ratio r/t. If the ratio r/t is kept constant, the porosity will be the same. Some mesochannel radii and wall thickness values used in this paper are listed in Table 2 for analysis. The thermal conductivities with different porosities are shown in Fig. 4. And the results of our previous work, molecular-dynamic (MD) simulated thermal conductivities[31] of a mesoporous silicas (MCM-41) with a similar structure are also shown in Fig. 4 for comparison.

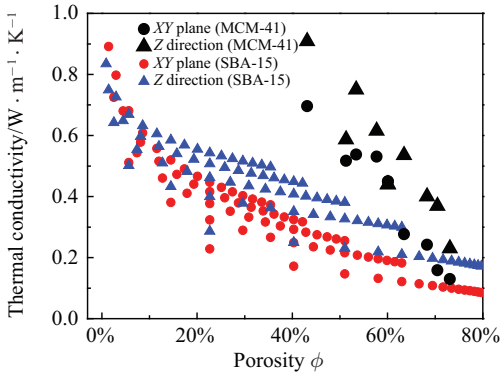


Fig. 4. (color online) Lattice thermal conductivities of the mesoporous silicas at $T = 300$ K with different porosities.

Table 2. Porosities at different mesochannel radii and wall thickness values.

Porosity t/nm / r/nm	1	3	5	7
2	40.3%	14.5%	7.4%	4.5%
6	66.6%	40.3%	27.0%	19.3%
10	75.0%	53.7%	40.3%	31.4%
14	79.0%	61.5%	49.2%	40.3%

With the increase of porosity, the thermal conductivity of the mesoporous silica decreases not strictly linearly, but in a manner similar to the tendency of the MD simulation result as shown in Fig. 4. This is interpreted by the fact that the same porosity can correspond to different mesochannel radii and wall thickness values, such as $\phi = 40.3\%$ (in shadow) shown in Table 2. Thermal conductivities of the mesoporous silica with $\phi = 40.3\%$ are further shown in Fig. 5 to illustrate the phenomenon. Figure 5 shows that the thermal conductivity increases with wall thickness and mesochannel radius rising while the porosity remains constant. However, the result in this paper is much lower than the MD simulation result. It can be interpreted by the fact that the thermal conductivity varies with the density according to a power law

relationship,[32,33] the theoretical thermal conductivity calculated with density $\rho = 2.2\ \mathrm{g\cdot cm^{-3}}$ is lower than that predicted by the MD simulation method with $\rho = 2.66\ \mathrm{g\cdot cm^{-3}}$, and additionally, thermal conductivities predicted by the MD simulation method employing solid wall boundary conditions are possibly higher than the actual values.[34]

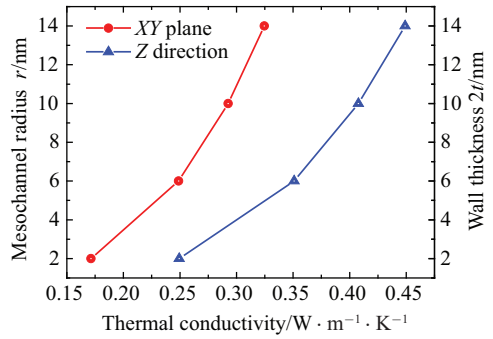


Fig. 5. (color online) Lattice thermal conductivities of the mesoporous silicas with porosity $\phi = 40.3\%$ at $T = 300$ K.

5. Discussion of the effective thermal conductivity

The effective thermal conductivity (ETC) model[31] described by our previous work, which is based on the one-dimensional heat transfer, is used here to take into account both the shell and the confined air in a mesochannel. The ETCs of the mesoporous silicas with different porosities are studied as shown in Fig. 6. The one-dimensional reference bar method and the corresponding instrument described by our previous work[35] are adopted to measure the ETC of the powder sample of SBA-15. The experimental results are shown in Fig. 6 for comparison. Although the SBA-15 particle is anisotropic, the powder sample is thought to be isotropic. The direction-averaged values of the calculated ETCs are further obtained as shown by the curve in Fig. 6.

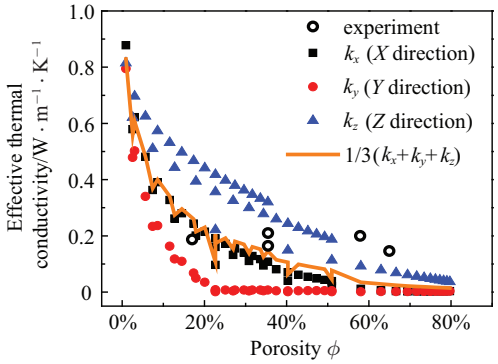


Fig. 6. (color online) Theoretical and experimental effective thermal conductivities of the mesoporous silicas with different porosities.

The deviation of the theoretical result from the experimental one is obvious at the large porosity scale. It may be interpreted by the fact that the thermal radiation becomes the main thermal transfer mode at the large porosity scale, but it was not considered in the calculation. The predicted ETCs of SBA-15 with only conduction considered are quite low at the large porosity, even lower than the thermal conductivity of the silica aerogel ($k = 0.017\ \mathrm{W\cdot m^{-1}\cdot K^{-1}}$ [36]). To realize it, doping carbon or other matters which can strongly absorb infrared light into SBA-15 is one possible way, similar to doping the carbon into aerogel.[36,37]

The fluctuations of the calculated ETCs in Fig. 6 are caused by the fact that the same porosity can correspond to different values of mesochannel radius and wall thickness, as discussed in Section 4. In addition, compared with the thermal conductivity of the shell (shown in Fig. 4), the ETC of the SBA-15 is smaller and the anisotropic characteristic of the ETC is more obvious.

6. Conclusions

In this paper, the shell thermal conductivity of the mesoporous silica (SBA-15) is first studied by the theoretical investigation under the relaxation time approximation. A one-dimensional heat transfer model developed by our previous work is used to predict the ETC of the mesoporous silica. The experimental results of the ETC are also given for comparison. The shell thermal conductivity of the mesoporous silica decreases with mesochannel radius increasing or wall thickness decreasing, does not strictly decrease with porosity rising. The shell thermal conductivity increases with wall thickness and mesochannel radius increasing, with the porosity kept unchanged. The predicted ETC of SBA-15, without thermal radiation considered, is quite low at the large porosity. The SBA-15 doped with carbon or other matters which can strongly absorb infrared light possibly has an ultra-low ETC.

References

[1] Fesmire J E and Sass J P 2008 *Cryogenics* **48** 223
[2] Fesmire J E 2006 *Cryogenics* **46** 111
[3] Sopian K, Zulkifli R, Sahari J and Othman M Y 2002 *J. Mater. Process. Technol.* **123** 179
[4] Nagoga G P, Anurov Yu M and Belousov A I 1986 *J. Eng. Physic. Thermophysics* **51** 884
[5] Yamamoto K, Sunagawa Y, Takahashi H and Muramatsu A 2005 *Chem. Commun.* **0(3)** 348
[6] Wang Z, Xie Y and Liu C 2008 *J. Phys. Chem. C* **112** 19818
[7] Sasidharan M, Mal N K and Bhaumik A 2007 *J. Mater. Chem.* **17** 278
[8] Zhang W, Cui J, Tao C, Lin C, Wu Y and Li G 2009 *Langmuir.* **25** 8235
[9] Coquil T, Richman E K, Hutchinson N J, Tolbert S H and Pilon L 2009 *J. Appl. Phys.* **106** 034910
[10] Choi S G, Ha T J, Yu B G, Jaung S P, Kwon O and Park H H 2008 *Ceram. Int.* **34** 833
[11] Yang C, Liu P, Ho Y, Chiu C and Chao K 2003 *Chem. Mater.* **15** 275
[12] Melero J A, Stucky G D, van Grieken R and Morales G 2002 *J. Mater. Chem.* **12** 1664
[13] Zhao D, Sun J, Li Q and Stucky G D 2000 *Chem. Mater.* **12** 275
[14] Han Y J and Klemens P G 1993 *Phys. Rev. B* **48** 6033
[15] Callaway J 1959 *Phys. Rev.* **113** 1046
[16] Balandin A and Wang K L 1998 *Phys. Rev. B* **58** 1544

[17] Klemens P G 1958 *Solid State Physics* ed. Seitz F and Turnbull D (New York: Academic) p. 1
[18] Klemens P G 1997 in *Chemstry and Physics of Nanostructures and Related Non-Equilibrium Materials*, ed. Ma E, Fultz B, Shall R, Morral J and Nash P (Warrendale: Minerals, Metals, & Materials Society) p. 97
[19] Lu X, Chu J H and Shen W Z 2003 *J. Appl. Phys.* **93** 1219
[20] Zou J and Balandin A 2001 *J. Appl. Phys.* **89** 2932
[21] Stephens R B 1973 *Phys. Rev. B* **8** 2896
[22] Zarzycki J 1982 *Les Verres et l'E' tat Vitreux* (Paris: Masson), and references therein
[23] Jund P and Jullien R 1999 *Phys. Rev. B* **59** 13707
[24] Khitun A, Balandin A and Wang K L 1999 *Superlatt. Microstruct.* **26** 181
[25] Huang W Q, Chen K Q, Shuai Z, Wang L L and Hu W Y 2005 *Int. J. Mod. Phys. B* **19** 1017
[26] Galarneau A, Cambon H, Renzo F D, Ryoog R, Choib M and Fajula F 2003 *New J. Chem.* **27** 73
[27] Williams Q, Hemley R J, Kruger M B and Jeanloz R 1993 *J. Geophys. Res.* **98** 22157
[28] Cahill D G and Pohl R O 1987 *Phys. Rev. B* **35** 4067
[29] Horbach J, Kob W and Binder K 1999 *J. Phys. Chem. B* **103** 4104
[30] Zeller R C and Pohl R O 1971 *Phys. Rev. B* **4** 2029
[31] Huang C, Feng Y, Zhang X, Wang G and Li J 2011 *Acta Phys. Sin.* **60** 114401 (in Chinese)
[32] Ross R G, Andersson P, Sundqvist B and Backstrom G 1984 *Rep. Prog. Phys.* **47** 1347
[33] Jain A, Rogojevic S, Ponoth S, Gill W N, Plawsky J L, Simonyi E, Chen S T and Ho P S 2002 *J. Appl. Phys.* **91** 3275
[34] Chantrenne P and Barrat J L 2004 *J. Heat Transfer* **126** 577
[35] Huang C, Feng Y, Zhang X, Li W, Yang M, Li J and Wang G 2012 *Acta Phys. Sin.* **61** 154402 (in Chinese)
[36] Fricke J and Tillotson T 1997 *Thin Solid Films* **297** 212
[37] Wei G, Liu Y, Zhang X, Yu F and Du X 2011 *Int. J. Heat Mass Transfer* **54** 2355